Journal of Alloys and Compounds 512 (2012) 190–194

Contents lists available at SciVerse ScienceDirect

Journal of Alloys and Compounds

journal homepage: www.elsevier.com/locate/jallcom

Preparation and properties of multifunctional Fe@C@Y_2O_3:Eu^{3+} nanocomposites

Jingxing Yang, Xuwei Yang, Hua Yang*

College of Chemistry, Jilin University, Changchun 130012, China

ARTICLE INFO

Article history:
Received 5 July 2011
Received in revised form
20 September 2011
Accepted 20 September 2011
Available online 24 September 2011

Keywords:
Core–shell structure
Magnetic
Luminescent
Multifunctional
Fe@C@Y2O3:Eu^{3+}

ABSTRACT

Multifunctional Fe@C@Y_2O_3:Eu^{3+} nanocomposites were prepared by the solvo thermal method, and their structure, magnetic and luminescent properties were characterized by X-ray diffraction (XRD), vibrating sample magnetometer (VSM) and scanning electron microscope (SEM). Results show that the nanocomposites are spherical with a mean diameter of 700 nm and there are high special saturation magnetization (47.4 emu/g) and strong red emission under UV-light. Even dispersed in water solution, the nanocomposites also exhibit a strong red emission under ultraviolet light radiation, and it could be manipulated using an external magnet. Thus it looks promising for application in biomedicine field, especially in drug targeting and fluorescence label. And we also discussed the effect of the electron transfer process between the Fe magnetic core and Y_2O_3:Eu^{3+} shell.

1. Introduction

During the past years, multifunctional magnetic core–shell nanoparticles [1] have attracted increasing attention due to their various applications in biological and chemical fields such as catalysis [2], magnetic resonance imaging [3], enzyme and protein immobilization [4], target-drug delivery [5], clinical diagnosis [6] and magnetic biological separation [7].

Recently, several outstanding efforts have been contributed to the development of magnetic@luminescent nanocomposites [8]. For example, Wang et al. [9] have successfully synthesized superparamagnetic fluorescent Fe_3O_4/ZnS core–shell and hollow nanospheres with diameters of <100 nm using a simple method that they called corrosion-aided Ostwald ripening. Yang et al. [10] and Gai et al. [11] have modified Fe3O4@ $nSiO_2$@$mSiO_2$ with luminescent YVO_4:Eu^{3+} to prepare magnetic, mesoporous and nanocomposites with core–shell-structure as drug carriers. Wang et al. [12] have fabricated Fe_3O_4@LaF_3:Ce^{3+}, Tb^{3+} bifunctional composites with a layer-by-layer technology. Ma et al. [13] have prepared bifunctionalization of magnetic Fe_3O_4@Y_2O_3:Eu^{3+} nanocomposites.

Up to date, the templating strategy is a common method for preparing magnetic core–shell nanoparticles. To the best of our knowledge, there are some reports about the nanocomposites as the core of Fe_3O_4 and as the shell of silica or polymer [14,2], but few reports about the nanocomposites as the magnetic core of the metal Fe. For protecting the core of the composite, the shell of the composite is coated on the surface of the core of the composite. The compounds of the shell must be chemical and colloidal stability in acid or alkali solution, but the silica and the polymer cannot be satisfied this requirement absolutely. Thus, the development of a suitable compound for the shell particle has become a pressing need. For Fe_3O_4@C nanocomposites, this difficult problem is solved. The carbon has many excellences: not only it is stable in acid or alkali solution, but also is easy to introduce activated groups onto the carbon layer. Furthermore, after calcinated Fe_3O_4 was deoxidized to metal Fe at N_2, this can be improved magnetic properties of the nanocomposites. As a result, the activated groups on the carbon layer could be given rise to preferred sites of nucleation [15]. Multifunctional nanocomposites could be fabricated by connecting other functional groups to the activated sties [16]. In the reported researches, the general used fluorescent materials are quantum dots (QDs) and organic dyes. However, QDs are less chemically stable, potentially toxic, and show fluorescence intermittence, and the organic dyes exhibit photobleaching and low fluorescence quantum yield. Thus, such disadvantages hinder their application used in human body [17,18].

In this paper, we designed a facile approach for fabricating multifunctional magnetic, luminescent Fe@C@Y_2O_3:Eu^{3+} nanocomposites with core–shell-structure. For the middle carbon layer, there are four functions: (1) protecting Fe as the core from oxidizing; (2) avoiding Fe_3O_4 deoxidized to metal Fe after calcination for improve magnetic property of the nanoparticles; (3) decreasing fluorescence quenching effect of the nanocomposites by Fe as the cores and (4) providing activated groups to modify on the surface of the Fe core with luminescent phosphors.

* Corresponding author.
E-mail address: huayang86@sina.com (H. Yang).

0925-8388/$ – see front matter © 2011 Elsevier B.V. All rights reserved.
doi:10.1016/j.jallcom.2011.09.061

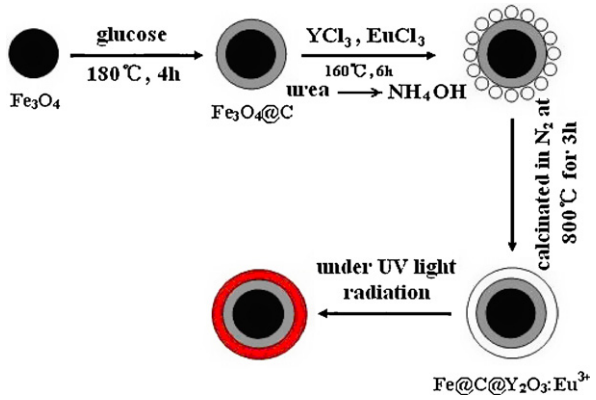

Scheme 1. Formation process of the multifunctional Fe@C@Y_2O_3:Eu^{3+} nanoparticles.

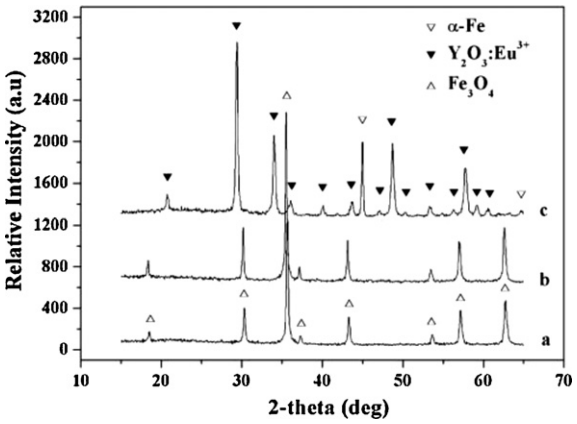

Fig. 1. XRD patterns of Fe_3O_4 (a), Fe_3O_4@C (b) and Fe@C@Y_2O_3:Eu^{3+}(c).

The nanocomposites exhibit favorable magnetic and luminescent properties. This nanocomposite has potential applications in biomedicine and biochemistry field, such as target-drug delivery and luminescence label.

2. Experimental procedures

2.1. Chemicals and materials

Ferric chloride crystal ($FeCl_3{\cdot}6H_2O$), polyethylene glycol (PEG, MW 10000), glucose ($C_6H_{12}O_6{\cdot}H_2O$), yttrium oxide (Y_2O_3, 99.99%), europium oxide (Eu_2O_3, 99.99%), hydrochloric acid (HCl), urea ($(NH_2)_2CO$) were purchased from Beijing Chemical Works, and Sodium acetate ($CH_3COONa{\cdot}3H_2O$), ethanol absolute and ethylene glycol (EG) were purchased from Tianjin Tiantai Chemical Reagent. The starting material and other reagents were analytical grade and used without any further purification.

2.2. Synthesis of core–shell Fe@C@Y_2O_3:Eu^{3+} microspheres

2.2.1. Hydrothermal synthesis of Fe_3O_4@C microspheres

The Fe_3O_4 particles were synthesized through a solvothermal method according to the reported method [19]. $FeCl_3{\cdot}6H_2O$ (1.35 g, 5 mmol), NaAc·$3H_2O$ (5.56 g) and PEG (1.0 g) were dissolved in EG (40 ml) to form a mixture solution, transferred into a Teflon-lined stainless-steel autoclave with a capacity of 50 ml. The autoclave was heated at 200 °C for 8 h, washed with distilled water and ethanol, and then dried at 50 °C for 12 h to prepare Fe_3O_4 powder. Fe_3O_4 (1.0 g) powder was dispersed in 0.5 M glucose aqueous solution, then transferred into the autoclaves and heated at 200 °C for 4 h, washed with distilled water and ethanol, then dried at 50 °C for 12 h to prepare Fe_3O_4@C microspheres.

2.2.2. Solvothermal synthesis of Fe@C@Y_2O_3:Eu^{3+} microspheres

Y_2O_3 and Eu_2O_3 were first co-added into the equal stoichiometric amount HCl solution to form YCl_3 and $EuCl_3$ mixture solution in which molar ratio of Y/Eu was 9:1. Fe@C powder and urea were added to the mixture solution under magnetic stirring to form the suspension. After ultrasonicated for 30 min, the suspension was transferred into a 50 mL capacity Teflon-lined stainless-steel autoclave. The autoclave was heated at 160 °C for 6 h, and then cooled to room-temperature naturally to prepare the precursor. The precursor was washed with distilled water for several times, dried at 50 °C for 12 h and calcinated in a nitrogen gas (N_2) atmosphere at 800 °C for 3 h to prepare Fe@C@Y_2O_3:Eu^{3+} microspheres.

2.3. Characterization

The crystal phase and purity of the microspheres were characterized by X-ray powder diffraction (XRD-6000, SHIMADZU, Japan) equipped with graphite monochromatized Cu Kα radiation (λ=1.54056 Å), employing a scanning rate of 6° min^{-1}, in the 2θ range from 15° to 65°. The micromorphologies of the as-prepared samples were inspected by scanning electron microscopy (SEM, Philip XL30, Holand). The vibrating sample magnetometer (VSM) was used for magnetic measurement at room temperature, and a spectrophotometer (Hitachi F-4500 spectrouorimeter equipped with a 150 W xenon lamp as the excitation source) was used for the photoluminescent (PL) measurement.

3. Results and discussion

The formation process of the multifunctional nanoparticles is presented in Scheme 1. To be brief, the Fe_3O_4 nanoparticles were synthesized by a solvothermal method according to the reported method [19]. Subsequently, the Fe_3O_4 microspheres were treated by carbon-coated procedure, to result in the formation of the Fe_3O_4@C microspheres with an amorphous carbon layer. Finally, photoluminescent Y_2O_3:Eu^{3+} layer was deposited on the surface of the Fe_3O_4@C microspheres by a hydrothermal process and a calcinating procedure. The as-prepared Fe@C@Y_2O_3:Eu^{3+} can exhibit a strong red emission under UV light radiation. Detailed experimental processes are given in Section 2.

Fig. 1a shows the X-ray diffraction pattern of the as-synthesized Fe_3O_4 microspheres. Compared with the data in JCPDS No. 85-1436, all peaks in the patterns (marked with △) can be indexed to a face-centered cubic structure of magnetite. Fig. 1b is the XRD pattern of the Fe_3O_4@C microspheres. Because this process was reacted at 200 °C, the diffraction peak of the amorphous carbon layer coated on the surface of the Fe_3O_4 cannot be seen from Fig. 1b. And Fig. 1c is the XRD pattern of the Fe@C@Y_2O_3:Eu^{3+} nanocomposites. In this pattern, magnetic nanocomposites exhibit the characteristic diffraction peaks of Y_2O_3 with cubic structure and additional peaks that coincide with the peaks of body-centered cubic α-Fe. The strong diffraction peak at 44.9° and weak peak at 64.7° are the characteristic (1 1 0) and (2 0 0) diffractions of body-centered cubic α-Fe. This indicated that the Fe_3O_4 has been deoxidized to face-centered cubic α-Fe by amorphous carbon and the Y_2O_3:Eu^{3+} was single-phase with body-centered cubic structure. Besides above peaks, no other impure phase peaks showed in Fig. 1c.

The morphologies of Fe_3O_4 and Fe@C@Y_2O_3:Eu^{3+} nanopaticles were analyzed by SEM in Fig. 2. From Fig. 2A, it can be seen that the Fe_3O_4 particles were typical spherical with diameter size from 300 nm to 400 nm, excluding agglomerate particles, and there are some rough porous on the surface of the particles. Furthermore, the shape and size of Fe_3O_4 particles were not very uniform, resulted from reactive time and reactive concentration to influence the morphology and diameter of the nanocomposites [19] in a typical solvothermal process. Fig. 2B shows the SEM image of the prepared Fe@C@Y_2O_3:Eu^{3+} nanoparticles. It is indicated that the shape of nanoparticles is almost spherical, their particle size is about 700 nm and there are some agglomerates. Compared with Fe_3O_4 particle in Fig. 2A, there are some porous and more smooth on the surface of Fe@C@Y_2O_3:Eu^{3+} composite because Fe_3O_4 nanocrystals disappeared and the particle size increased. This indicates that the core materials coated by the shell materials.

Fig. 3 is the digital photos of the as-prepared Fe@C@Y_2O_3:Eu^{3+} nanocomposites dispersed in distilled water. The photos A and C are without external magnetic field, and The photos B and D are under external magnetic field. Analogously, A and B are the

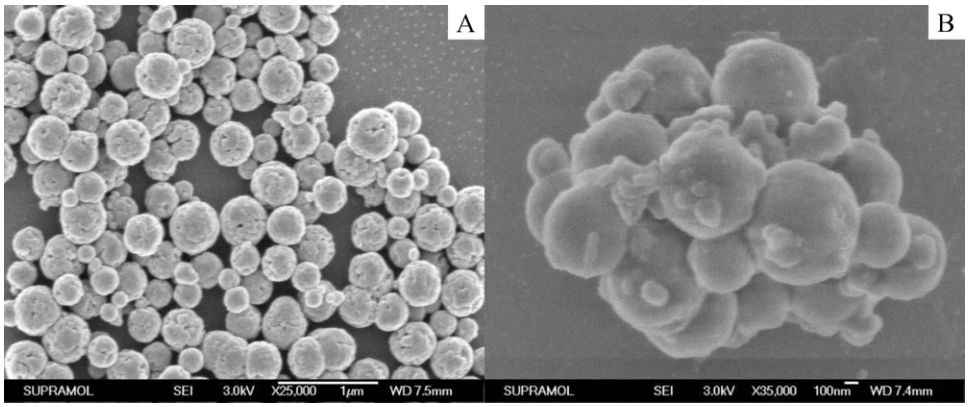

Fig. 2. SEM images of Fe_3O_4 (A) and Fe@C@Y_2O_3:Eu^{3+} (B) microspheres.

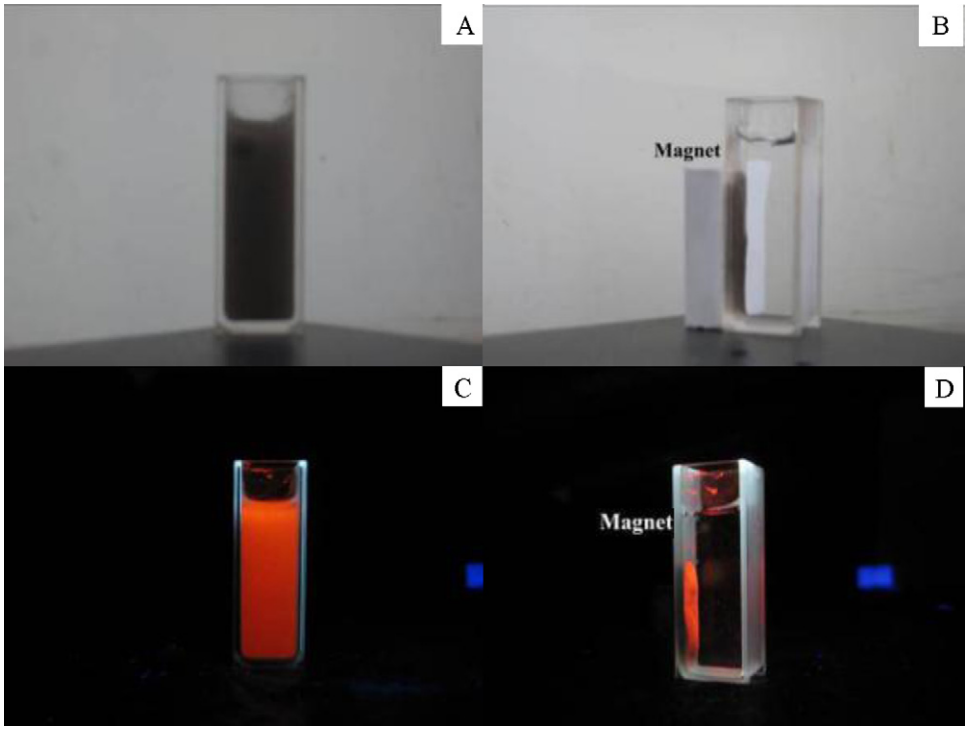

Fig. 3. Digital photos of Fe@C@Y_2O_3:Eu^{3+} nanocomposites without external magnetic field (A and C) and ultraviolet light radiation (A and B), under external magnetic field (B and D) and ultraviolet light radiation (C and D).

photos without ultraviolet light radiation, and C and D are the ones under ultraviolet light radiation. From A and C, it can be seen that the nanocomposites can be homogeneously dispersed in water solution very well, and even dispersed in water solution they also exhibit a strong red emission under ultraviolet light radiation (shows in Fig. 3C). Moreover from B and D, the nanocomposites show fast response to the external magnetic field: when putting a magnet on one side of the sample cell, all of the homogeneous dispersed samples moved to the side near the magnet in several seconds, which suggests that the composites exhibit excellent magnetic responsivity. When ultraviolet light radiation was performed, bright red light could only be observed at the corresponding place near the magnet (shows in Fig. 3D), indicating that nearly all the Y_2O_3:Eu^{3+} nanoparticles have been combined with magnetic Fe@C nanoparticles. Moreover, because of their high magnetization, the digital photos of the Fe@C@Y_2O_3:Eu^{3+} nanocomposites suggest its excellent magnetic responsivity and redispersibility.

Fig. 4 shows the excitation (left) and emission (right) spectra of the samples. Fig. 4a is the excitation spectra of Y_2O_3:Eu^{3+} (λ_{em} = 610 nm). Obviously, it can be seen that the excitation spectrum consists of a broadband with a maximum at 260 nm due to the charge-transfer band (CTB) between O^{2-} and Eu^{3+} and multiple f–f transition lines of Eu^{3+} (assigned in Fig. 4a) in the longer wavelength region [20]. Fig. 4b is the excitation spectra of Fe@C@Y_2O_3:Eu^{3+} (λ_{em} = 610 nm). Only the Eu^{3+}–O^{2-}CTB can be seen, but the f–f transition lines of Eu^{3+} can hardly be seen. Fig. 4c and d are the emission spectra of Y_2O_3:Eu^{3+} (λ_{ex} = 254 nm) and Fe@C@Y_2O_3:Eu^{3+} (λ_{ex} = 254 nm). The typical emission spectrum of the $^5D_0 \rightarrow {}^7F_J$ (J = 0, 1, 2, 3, 4) transition lines of Eu^{3+}, with the $^5D_0 \rightarrow {}^7F_2$ hypersensitive transition (610 nm) being the most prominent peak (assigned in Fig. 4c). In Fig. 4b, comparing with Fig. 4a, the intensity of the excitation spectrums is weaker, not only the Eu^{3+}–O^{2-}CTB but also the f–f transition lines of Eu^{3+}. But it is hardly to observe the excitation spectrums of the f–f transition lines

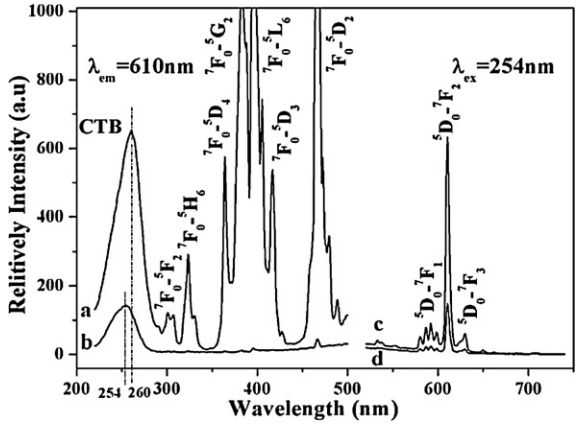

Fig. 4. Excitation spectra and emission spectra of Y_2O_3:Eu^{3+} (a and c) and Fe@C@Y_2O_3:Eu^{3+} (b and d).

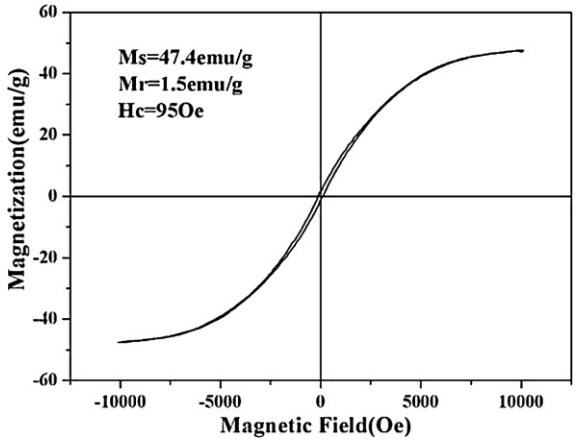

Fig. 6. The magnetic hysteresis loop of Fe@C@Y_2O_3:Eu^{3+} nanocomposite.

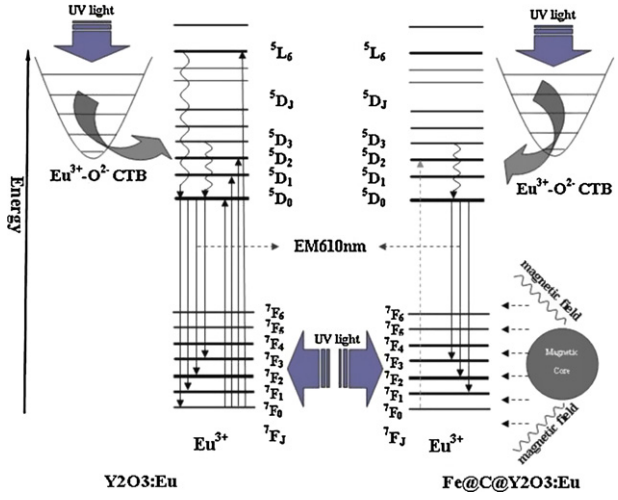

Fig. 5. The mechanism map of magnetic core's quenching effect in Fe@C@Y_2O_3:Eu^{3+} composites.

of Eu^{3+} from Fig. 4b. We think it is resulted from the magnetic core's quenching effect.

Fig. 5 shows the mechanism of the magnetic core's quenching effect in Fe@C@Y2O3:Eu^{3+} nanocomposite. The magnetic field produced by the magnetic core limits the 4f electrons of the Eu^{3+} to transfer from ground state to excitation state, which makes the f–f transition ($^7F_0 \rightarrow {}^5D_J$ and $^7F_0 \rightarrow {}^5L_6$ transition) of Eu^{3+} to become spin-forbidden transition. But the Eu^{3+}–O^{2-}CTB is due to the charge transition between the activator (Eu^{3+}) and the surrounding ligand (O^{2-}). When the host materials are absorbed energy, the electrons in the materials are transferred from the full molecular orbital of the ligand (O^{2-}) to the 4f energy level of the activators (Eu^{3+}). This progress cannot be affected by the magnetic field from the Fe core. In comparison, when the activators absorbed energy, the electron transitions will be taken place between the unfilled f energy levels. But the magnetic field limits the movement of the lone pair electron, consequently makes the f–f transition of Eu^{3+} to become spin-forbidden transition. We think that the quenching effect of the magnetic core towards the f–f electron transition of Eu^{3+} is stronger than the effect towards the Eu^{3+}–O^{2-}CTB.

Fig. 6 shows the magnetic hysteresis loop of the Fe@C@Y_2O_3:Eu^{3+}. The special saturation magnetization value M_s, the remanent magnetization M_r and the coercivity H_c of Fe@C@Y_2O_3:Eu^{3+} are 47.4 emu/g, 1.5 emu/g and 95 Oe, respectively. It should be noted that, in despite of being coated by two shells, the multifunctional nanocomposite also shows strong magnetic performance, which suggests its suitability for magnetic separation and targeting [21].

4. Conclusions

In summary, Fe@C@Y_2O_3:Eu^{3+} nanocomposites with magnetic and luminescent properties were successfully synthesized by two-step process. It is shown that the morphology of the nanocomposites is a spherical morphology, a mean particle size is about 700 nm, and there are high special saturation magnetisation M_s (47.4 emu/g) and strong red emission under UV-light. The Fe@C@Y_2O_3:Eu^{3+} nanocomposites have high magnetic performance and excellent photoluminescent properties. Even dispersed in water solution, the nanocomposites also exhibit a strong red emission under ultraviolet light radiation, and it could be manipulated using an external magnet. Such multifunctional nanocomposite may find many biomedical applications, such as cancer detection and drug delivery.

Acknowledgement

This work is supported by the National Natural Science Foundation of China (NSFC).

References

[1] Y. Li, G. Chen, Q. Li, G. Qiu, X. Liu, J. Alloys Compd. 509 (2011) 4104–4107.
[2] Z. Wang, S. Zhu, S. Zhao, H. Hu, J. Alloys Compd. 509 (2011) 6893–6898.
[3] H. Yang, X. Li, H. Zhou, Y. Zhuang, H. Hu, H. Wu, S. Yang, J. Alloys Compd. 509 (2011) 1217–1221.
[4] T. Iwasaki, N. Sato, K. Kosaka, S. Watano, T. Yanagida, T. Kawai, J. Alloys Compd. 509 (2011) L34–L37.
[5] K. Kai Chen, P.S. Conti, Adv.Drug Deliv. Rev. 62 (2010) 005–1022.
[6] Q. Zhang, Q. Xiao, Z. Lin, X. Ying, Z. Li, J.-M. Lin, Clin. Biochem. 43 (2010) 1003–1008.
[7] J. Hu, M. Xie, C.-Y. Wen, Z.-L. Zhang, H.-Y. Xie, A.-A. Liu, Y.-Y. Chen, S.-M. Zhou, D.-W. Dai-Wen Pang, Biomaterials 32 (2011) 1177–1184.
[8] H. Peng, G. Liu, X. Dong, J. Wang, J. Xu, W. Yu, J. Alloys Compd. 509 (2011) 6930–6934.
[9] Z.X. Wang, L.M. Wu, M. Chen, S.X. Zhou, J. Am. Chem. Soc. 131 (2009) 11276–11277.
[10] P.P. Yang, Z.W. Quan, Z.Y. Hou, C.X. Li, X.J. Kang, Z.Y. Cheng, J. Lin, Biomaterials 30 (2009) 4786–4795.
[11] S.L. Gai, P.P. Yang, C.X. Li, W.X. Wang, Y.L. Dai, N. Niu, J. Lin, Adv. Funct. Mater. 20 (2010) 1166–1172.
[12] L.Y. Wang, Z.H. Yang, Y. Zhang, L. Wang, J. Phys. Chem. C 113 (2009) 3955–3959.
[13] Z.Y. Ma, D. Dosev, M. Nichkova, S.J. Gee, B.D. Hammockb, I.M. Kennedy, J. Mater. Chem. 19 (2009) 4695–4700.

[14] E. Karaoğlu, A. Baykal, H. Deligöz, M. Şenel, H. Sözeri, M.S. Toprak, J. Alloys Compd 509 (2011) 8460–8468.
[15] Y.A. Barnakov, M.H. Yu, Z. Rosenzweig, Langmuir 21 (2005) 7524.
[16] L. Zhang, W.Z. Wang, M. Shang, S.M. Sun, J.H. Xu, J. Hazard. Mater. 172 (2009) 1193–1197.
[17] D.B. Mawhinney, V. Naumenko, A. Kuznetsova, J.T. Yates, J. Liu, R.E. Smalley, J. Am. Chem. Soc. 122 (2000) 2383–2384.
[18] M. Terashima, M. Uchida, H. Kosuge, P.S. Tsao, M.J. Young, S.M. Conolly, T. Douglas, M.V. McConnell, Biomaterials 32 (2011) 1430–1437.
[19] H. Deng, X.l. Li, Q. Peng, X. Wang, J.P. Chen, Y.d. Li, Angew. Chem. Int. Ed. 44 (2005) 2782–2785.
[20] J. Yang, Z.W. Quan, D.Y. Kong, X.M. Liu, J. Lin, Cryst. Growth Des. 7 (2007) 730–735.
[21] M.F. Zhang, S.G. Shi, J.X. Meng, X.Q. Wang, H. Fan, Y.C. Zhu, X.Y. Wang, Y.T. Qian, J. Phys. Chem. C 112 (2008) 2825–2830.